

Enhancement of the weak scattered signal in apertureless near-field scanning infrared microscopy

Larissa Stebounova

Department of Chemistry, University of Pittsburgh, Pittsburgh, Pennsylvania 15260

Boris B. Akhremitchev

Department of Chemistry, Duke University, Durham, North Carolina 27708

Gilbert C. Walker^{a)}

Department of Chemistry, University of Pittsburgh, Pittsburgh, Pennsylvania 15260

(Received 24 February 2003; accepted 22 May 2003)

An interferometric method is used to enhance the weak scattered signal in apertureless near-field scanning infrared microscopy. The method involves introducing a homodyning reference field, and amplifies the desired signal field by the magnitude of the reference field. This method markedly improves the signal-to-noise ratio of the detected signal, over the nonhomodyned experiment. A model for the dependence of the near-field signal, as a function of the normal distance of the tip from the surface, is discussed. Application of a model in which the tip is represented by two spherical scatterers, one large and one small, indicates the electromagnetic field enhancement is 90-fold greater at the sharp apex of the metallic probe tip. © 2003 American Institute of Physics. [DOI: 10.1063/1.1592876]

I. INTRODUCTION

The highest resolution infrared microscopy is apertureless near-field scanning infrared microscopy (ANSIM). It uses a metallic, semiconductor, or dielectric probe as a scattering site for radiation in the immediate vicinity of the sample surface. Wessel is credited with proposing the apertureless probe technique.¹ The idea of this method is to perturb the electromagnetic field localized at the surface of a sample so that the decaying components of the field will propagate to a remote detector.² The tip is oscillated normal to the surface and scattered light is collected at harmonics of the oscillatory frequency. The spatial resolution obtained by this method can be at least an order of magnitude better than is obtained by the apertured probe technique.^{3–8} ANSIM has been reported at a lateral spatial resolution of $\lambda/300$ in the infrared,⁹ and $\lambda/100$ for the analogous measurement in the visible.¹⁰ This work has taken place along with notable developments in apertured near-field methods and other new optical and infrared microscopies.^{11–20}

In apertureless near-field IR microscopy, the development of several imaging techniques, including constant height imaging, detection of the scattered signal at higher harmonics of the tip motion, heterodyne detection, and homodyne detection,^{21–24} in addition to the availability of new IR, tunable sources, have set the stage for significant advances. One of the primary challenges in apertureless near-field microscopy is the detection of the weak scattered field. This article presents a solution to this problem, which is to homodyne the scattered field using a reference field. This provides a signal enhancement that scales as the reference

field amplitude, and also provides significant reduction of the time required to align the apparatus.

II. EXPERIMENTAL DETAILS

The scanning near-field microscope built in our laboratory (Fig. 1) is based on a commercial atomic force microscope (MultiMode AFM, Digital Instruments, Inc., Santa Barbara, CA). It uses a tunable carbon dioxide laser as the source of infrared light. The infrared light passes through a ZnSe partial (50/50) reflector (II-VI, Inc., Saxonburg, PA), and it is focused by means of a reflective objective (0.28 NA, Coherent, Inc., Auburn, CA) onto the end of a cantilever probe. Both reflective objective and partial reflectors are attached to an XYZ translational stage to assist in focusing the light. The probe is a commercial silicon probe (MikroMasch, Tallinn, Estonia) coated with 25 nm of platinum. The incident light is *p*-polarized light with an $\sim 80^\circ$ angle of incidence. The spot width is approximately 50 μm , and the radiation power is 20–100 mW. The beam from a He–Ne laser copropagates with the infrared beam, and it is used to visualize the path of infrared radiation. Infrared radiation back-scattered by the sample and the probe returns through the same reflective objective and partial reflectors. It is focused onto a MCT infrared detector (Graseby Infrared, Orlando, FL) using a paraboloidal mirror (effective focal length 127 mm, Janos Technology, Inc., Townshend, VT). The MCT detector is situated on a separate translational stage in order to adjust its position into the scattered light. The MCT detector signal contains the nonmodulated background signal (dc component) and the modulated signal at the frequency of cantilever oscillations and its harmonics (ac component). The weak scattered signal from the probe is amplified interferometrically. This optical setup is very similar to a Michelson

^{a)}Author to whom correspondence should be addressed; electronic mail: gilbertw@pitt.edu

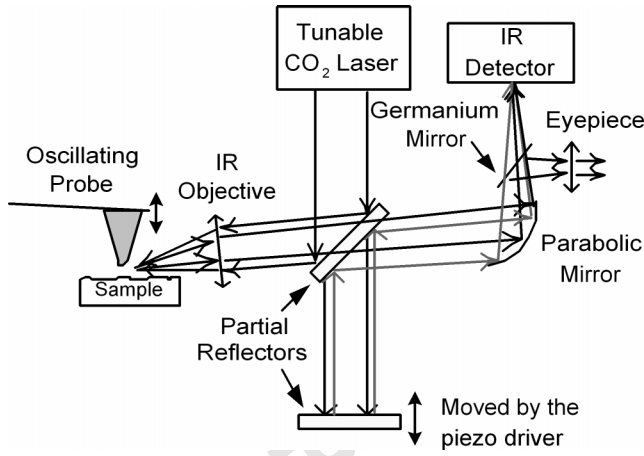


FIG. 1. Schematic representation of the apertureless near-field infrared microscope. The backscattered light, E_{sc} , is modulated by the oscillating tip. The piezodriver adjusts the relative phase of the homodyning reference field, E_r , that interferes at the detector with the light backscattered by the probe. The dominant ac contribution to the homodyned intensity at $2\langle E_{sc}E_r \rangle$ is detected using a lock-in amplifier.

interferometer. The partial reflector is placed onto a moving stage, which is driven by the piezodriver. The piezodriver has an automated phase feedback control, which is used to maximize the detected signal. The intensity of the reference beam was modified by inserting a partial reflector into the reference beam arm of the interferometer.

The ac component was amplified using a lock-in amplifier analyzing at twice the frequency of cantilever oscillation. A gold film (thickness ~ 20 nm) evaporated on a microscope coverslip was used as a substrate. The frequency of the incident light was ~ 950 cm^{-1} .

III. RESULTS AND DISCUSSION

The detection of the near-field signal is based on lock-in detection of the signal modulated by an oscillating probe tip at integer multiples of the frequency of the oscillation. This modulation is used to extract the near-field signal from the scattered background. It has been noted that the signal modulated at the fundamental frequency (Ω) of cantilever oscillation still contains a large contribution from the signals from different sources that are not surface specific.^{20,25} We use the detection of the near-field signal modulated at the harmonic (2Ω) of the probe oscillation in order to eliminate the background contribution.^{22,25,26} In some cases the detection of the scattered signal at the harmonics of the oscillation frequency is not sufficient to extract a truly optical signal. The use of homodyne or heterodyne detection is employed to remove an unwanted signal.²¹⁻²⁴ Our goal is to improve the signal-to-noise ratio by amplifying the weak near-field signal collected at the second harmonic of the oscillation frequency using homodyne detection.

Since we have interference of scattered and reference beams, the total intensity of the signal at the detector is

$$I_t = \langle (E_{sc} + E_r)^2 \rangle = \langle E_{sc}^2 \rangle + \langle E_r^2 \rangle + 2\langle E_{sc}E_r \rangle, \quad (1)$$

where E_{sc} is the scattered field and E_r is the reference field.

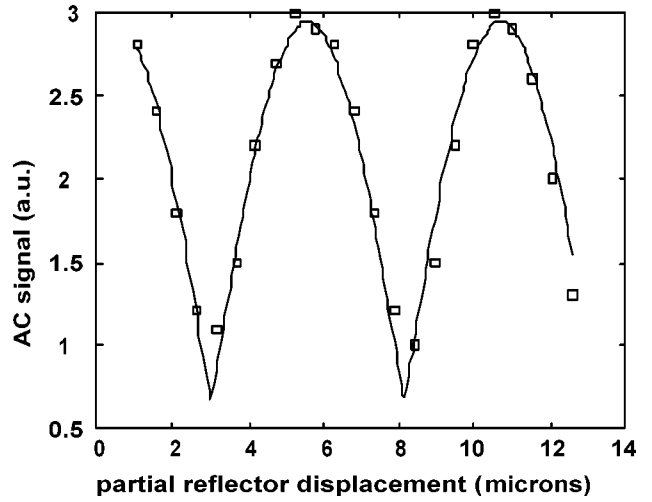


FIG. 2. Dependence of the near-field signal on displacement of the partial reflector. Squares represent the data points, the solid line represents the fit, whose functional form is the absolute value of cosine of the displacement.

Here is the expression for E_{sc} , which is modulated by the oscillating cantilever:

$$E_{sc} = A_1 [1 + C_1 \cos(\Omega t) + C_2 \cos(2\Omega t + \Phi)] \times \cos(\omega t + \varphi),$$

where A_1 is the amplitude of the nonmodulated scattered light, C_1 and C_2 are fractions of the first and second harmonics of the demodulated near-field signal, Φ is the relative phase of the second-harmonic signal, ω and φ are the frequency and the phase shift of the incident light, Ω is the frequency of cantilever oscillations, and we consider E_r in the form:

$$E_r = A_2 \cos(\omega t),$$

where A_2 is the amplitude of the reference signal, and ω is the frequency of the incident light, then the amplitude of the ac component of the signal at the 2Ω detection frequency is

$$AC = A_1^2 \left(\frac{C_1^2}{4} + C_2 \right) + A_1 A_2 C_2 \cos \varphi, \quad (2)$$

and the amplitude of the dc component of the detector signal is

$$DC = \frac{A_2^2}{2} + \frac{A_1^2}{4} (2 + C_1^2 + C_2^2) + A_1 A_2 \cos \varphi. \quad (3)$$

Since amplitude A_1 is much less than A_2 and fractions C_1 , C_2 are small, we can neglect the first term in Eq. (2) and the second term in Eq. (3). The phase shift φ between the reference and scattered beams is adjusted to maximize the signals using automated phase feedback control. Figure 2 shows how the ac component depends on the phase shift. The phase feedback uses the lock-in amplifier in order to monitor the deviations of the signal from its maximum position. The relative phase of the reference beam reflector is modulated by oscillating the position of the reflector with a piezoelement at a frequency of 10 Hz and with ~ 500 nm peak-to-peak amplitude. The effect of such modulation on the 2Ω component is detected with another lock-in amplifier operating at the

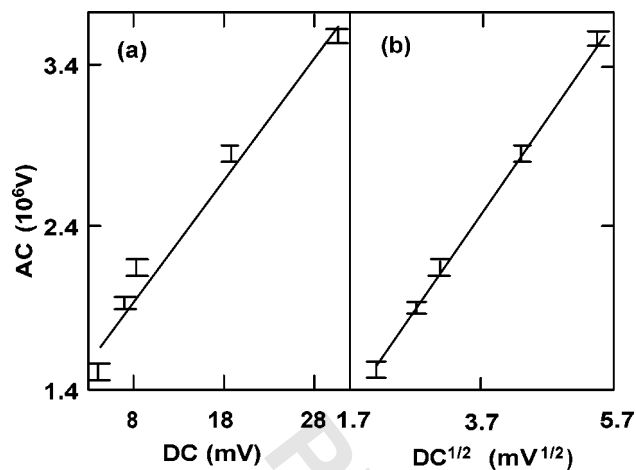


FIG. 3. Amplitude of scattered near-field signal at 2Ω vs (a) amplitude of dc component and (b) square root of the amplitude of dc component. Solid lines represent a linear fit to the data points.

frequency of the position modulation. The demodulated output is used as a feedback signal of the custom-built piezodriver. The piezodriver moves the reflector in order to zero the feedback signal, and hence, to maximize the ac signal. Such motion occurs on a time scale of several seconds and it does not affect data collected within one scan line. Slow variations in the phase of the reference beam due to, e.g., thermal drift, are compensated. The amplitude of the ac signal is proportional to the square root of the amplitude of the interferential dc component:

$$ac \propto \sqrt{dc}, \quad (4)$$

where ac is the ac component amplified by homodyne detection and dc is the dc component amplified by the homodyne detection dc component.

We collected the near-field signal at five different intensities of the reference signal. Both components were normalized by the intensity of the incident light. Data were collected at twice the frequency of the cantilever oscillations. Panel (a) in Fig. 3 shows the ac vs dc dependence. The linear fit does not correlate well with the data points. Panel (b) shows very good correlation between the data and the linear fit.

The distance dependencies of ac signals are presented in Fig. 4. The smallest two signals in panel (b) of Fig. 4 were collected without a reference beam. We note that even without the reference beam sometimes we could register a large 2Ω signal. Such a large signal can be explained by the interference of a weak modulated signal with a nonmodulated component, reflected from the sample-probe system (self-homodyning). There is no phase control of such a reflected beam and, therefore, the signal amplification is random. The signal represented by the dashed line was collected when self-homodyning did not occur; we cannot distinguish the signal from the noise in this case. When we add the reference beam to the system, without additional tuning of the apparatus we are able to see a strong ac signal. It is possible to see from Fig. 4 that we strongly amplify our scattered signal as the result of homodyne detection; the absolute value of the amplification depends on the presence of self-homodyning in

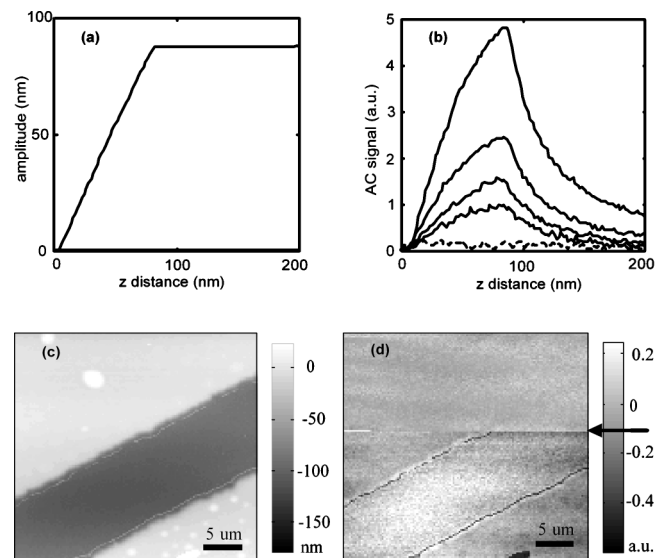


FIG. 4. Panel (a) shows the amplitude of cantilever oscillation vs the separation from the sample's surface. Panel (b) shows the amplitude of the scattered near-field signal demodulated at twice the frequency of the cantilever oscillation vs tip-sample separation for different intensities of the reference beam. The smallest two signals were obtained without a reference beam. The signal represented by the dashed line was collected when the apparatus was not tuned well. Panel (c) shows the height image of Si deposited onto a gold substrate. The bare gold may be seen as the dark, low-lying, central stripe. Panel (d) shows the apertureless near-field infrared image collected in two ways: in the top portion shows the signal was collected without benefit of homodyne amplification; in the bottom portion of the figure, beginning at a point indicated by the arrow, the signal was collected with homodyne amplification. The portion of the figure below the arrow is much clearer and exhibits a signal that is completely missing in the upper portion. This image demonstrates the value of homodyne amplification for infrared near-field microscopy.

the absence of the reference field. The control of the absolute value of amplification is illustrated in panels (a) and (b) of Fig. 4, while a more qualitative illustration may be seen in panels (c) and (d). The upper part of the near-field image in panel (d) shows that without homodyne amplification, the signal is weak and the image quality is poor (above arrow), but when the automating homodyning mechanism is activated (below arrow) the signal is stronger and the image quality is much improved. An explanation for the enhanced absorption by the small dots of silicon seen in panels (c) and (d) is beyond the scope of this article.

A. Polarizability of the tip-sample system and magnitude of the detected signal

Lock-in detection of the second-harmonic signal relies on the strong nonlinearity of the detected signal with respect to the probe's position above the sample. In our measurements the amplitude of the cantilever oscillation is comparable to the mean probe-sample distance, therefore, we cannot use the perturbation approach to predict the value of the lock-in detected signal. In order to apply an analytical model to explain the detected signal, we have to model the perturbation of the scattered radiation by the oscillating probe explicitly and use the results of such a model to generate a lock-in signal numerically. In our calculations, we considered the harmonic motion of the probe above the surface with amplitude A and mean probe-sample distance z_{mean} :

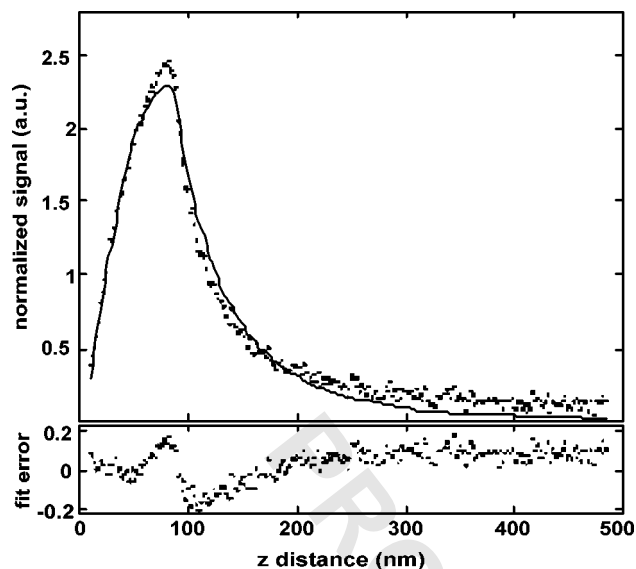


FIG. 5. Top panel shows the fit of the one scattering sphere model for the near-field signal. In the model, the sphere oscillates above the surface. The bottom panel shows the fit error.

$$z(t) = z_{\text{mean}} + A \times \cos(2\pi\Omega t). \quad (5)$$

Here, $z(t)$ is the distance (time dependent) of the probe above the surface and, Ω is the frequency of the cantilever oscillation. For each value of z_{mean} , corresponding amplitude was extracted from the amplitude versus distance dependence, collected simultaneously with the near-field signal. The values of the instantaneous probe position were used in a quasielectrostatic model²⁷ to calculate the time dependence of the effective polarizability for the oscillating probe-sample system. Because the real part of the permittivity of gold at $\sim 1000 \text{ cm}^{-1}$ is large, the quasielectrostatic model for p -polarized radiation from Ref. 27 can be simplified to

$$\alpha_{\text{eff}} = \frac{8\pi a^3}{1 - \frac{a^3}{4(a+z)^3}}, \quad (6)$$

where a is the radius of the probe, and z is the probe-sample separation. For each value of the mean probe-sample separation, the modulation in the polarizability due to the probe's oscillation was calculated. The intensity of the scattered radiation is proportional to the square of the polarizability.²⁸ Therefore, the homodyne-detected signal is proportional to the absolute value of polarizability. Lock-in detection of the second-harmonic signal was modeled by calculation of the numeric sine and cosine transforms of the polarizability versus time dependence at twice the frequency of the oscillating cantilever.

Our calculations indicate that such a model does not simultaneously explain the presence of the long-distance tail ($z > 100 \text{ nm}$) in the data, as shown in Fig. 5. This can be expected since our probe is not a nanometer-sized sphere but extends significantly further away from the surface. A second spherical scatterer, placed right above the first scatterer was included in the model in order to describe the shape of the probe more realistically (see the inset in Fig. 6). The near-field signal was calculated as a weighted sum of two terms,

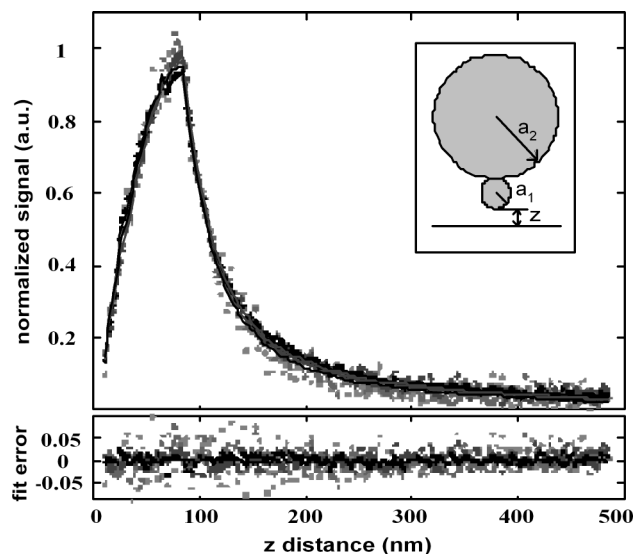


FIG. 6. Top panel shows the normalized near-field signal-distance dependence (dots) and curves calculated according to the model described in the text (solid lines). The bottom panel shows the fit error.

calculated according to Eq. (6) with different radii a . The fit parameters were these radii and the weight factors used in adding two terms. The model uses the same values of the radii for different experimental sets, the resulting values are 120 and 900 nm. Figure 6 shows the normalized data (points) and calculated dependence (solid lines) for three data sets with different level of reference beam intensity and one data set collected without the reference. The ratio of the scaling factors for two scatterers was 90 ± 10 , which can be explained by the enhancement of the electrical field near the sharp end of the probe (lightning rod effect²⁹).

The nearly perfect overlap of the curves in Fig. 6 indicates that the data collected without a reference beam were self-homodyned; light reflected back from the cantilever-sample system acted as a reference beam in this case. This explains why it is often difficult to tune an apparatus without the reference beam: overlap between relatively high intensity reflected radiation and the light scattered from the probe is required at the detector. With a reference beam there is a convenient means to control the back-reflected radiation. We note that Knoll and Keilmann²⁷ have previously reported the benefits of homodyne amplification in apertureless IR near-field scanning microscopy, where a lens was used to simultaneously adjust the focus and phase of a self-homodyning field. We believe our design brings the advantage of independent control of focus and phase in a reference field.

The noise calculated for the smallest ac signal, represented by dashed line in panel (b) of Fig. 4 is 0.034 a.u. The standard deviations from the fit to the described above model for the other four signals are in the range from 0.031 to 0.037 a.u. Thus, we can say that we fit distance dependencies well and the fit errors represent the noise level in the ac signals. Since the noise is almost the same for all signals in Fig. 4, and the signal without interferometric amplification is about 1:1, we conclude that signal-to-noise ratio is improved by as much as 150 times by utilizing interferometric amplification.

ACKNOWLEDGMENTS

The authors gratefully acknowledge support from ONR (N0001-02-D327) and NSF (CHE 9816820 and PHYS 0103048).

- ¹J. Wessel, *J. Opt. Soc. Am. B* **2**, 1538 (1985).
- ²A. Nemetz and A. Knoll, *J. Raman Spectrosc.* **27**, 587 (1996).
- ³A. Piednoir, C. Licoppe, and F. Creuzet, *Opt. Commun.* **129**, 414 (1996).
- ⁴A. Cricenti, *Appl. Surf. Sci.* **162**, 275 (2000).
- ⁵A. Lahrech, R. Bachelot, P. Gleyzes, and A. C. Boccara, *Opt. Lett.* **21**, 1315 (1996).
- ⁶Y. Inouye and S. Kawata, *Opt. Lett.* **19**, 159 (1994).
- ⁷C. A. Michaels, S. J. Stranick, L. J. Richter, and R. R. Cavanagh, *J. Appl. Phys.* **88**, 4832 (2000).
- ⁸B. Dragnea and S. R. Leone, *Int. Rev. Phys. Chem.* **20**, 59 (2001).
- ⁹B. Knoll and F. Keilmann, *Nature (London)* **399**, 134 (1999).
- ¹⁰F. Zenhausern, Y. Martin, and H. K. Wickramasinghe, *Science* **269**, 1083 (1995).
- ¹¹D. M. Adams, J. Kerimo, C. Y. Liu, A. J. Bard, and P. F. Barbara, *J. Phys. Chem. B* **104**, 6728 (2000).
- ¹²O. Cherniavskaya, S. Kaemmer, S. Schiering, J. Coffin, and D. M. Adams (unpublished).
- ¹³V. Deckert, D. Zeisel, R. Zenobi, and T. Vo-Dinh, *Anal. Chem.* **70**, 2646 (1998).
- ¹⁴D. A. Higgins, X. Liao, J. Hall, and E. Mei, *J. Phys. Chem. B* **105**, 5874 (2001).
- ¹⁵E.-S. Kwak, T. J. Kang, and D. A. Vanden Bout, *Anal. Chem.* **73**, 3257 (2001).
- ¹⁶H. F. Hamann, A. Gallagher, and D. J. Nesbitt, *Appl. Phys. Lett.* **73**, 1469 (1998).
- ¹⁷R. D. Schaller, J. C. Johnson, K. R. Wilson, L. F. Lee, L. H. Haber, and R. J. Saykally, *J. Phys. Chem. B* **106**, 5143 (2002).
- ¹⁸G. M. H. Knippels, T. I. Smith, H. A. Schwettman, and D. V. Palanker, *Opt. Commun.* **148**, 215 (1998).
- ¹⁹A. Zumbusch, G. R. Holtom, and X. S. Xie, *Phys. Rev. Lett.* **82**, 4142 (1999).
- ²⁰B. B. Akhremitchev, S. Pollack, and G. C. Walker, *Langmuir* **17**, 2774 (2001); B. B. Akhremitchev and G. C. Walker, *Bull. Chem. Soc. Jpn.* **75**, 1011 (2002).
- ²¹P. M. Bridger and T. C. McGill, *Opt. Lett.* **24**, 1005 (1999).
- ²²R. Hillebrand and F. Keilmann, *Phys. Rev. Lett.* **85**, 3029 (2000).
- ²³J. Azoulay, A. Debarre, A. Richard, and P. Tchenio, *Appl. Opt.* **39**, 129 (2000).
- ²⁴Y. Sasaki and H. Sasaki, *Jpn. J. Appl. Phys., Part 2* **39**, L321 (2000).
- ²⁵B. B. Akhremitchev, Y. Sun, L. Stebounova, and G. C. Walker, *Langmuir* **18**, 5325 (2002).
- ²⁶N. Maghelli, M. Labardi, S. Patane, F. Irrera, and M. Allegrini, *J. Microsc.* **202**, 84 (2001).
- ²⁷B. Knoll and F. Keilmann, *Opt. Commun.* **182**, 321 (2000).
- ²⁸C. F. Bohren and D. R. Huffman, *Absorption and Scattering of Light by Small Particles* (Wiley, New York, 1983).
- ²⁹A. Wokaun, *Solid State Phys.* **38**, 223 (1984).